Hindawi
Journal of Nanomaterials
Volume 2018, Article ID 6508061, 14 pages
https://doi.org/10.1155/2018/6508061

Research Article

Vibration Analysis of Bilayered Graphene Sheets for Building Materials in Thermal Environments Based on the Element-Free Method

Zhengtian Wu,[1] Yang Zhang,[2] Fuyuan Hu,[1] Qing Gao,[3] Xinyin Xu,[1] and Ronghao Zheng[4]

[1]*School of Electronic and Information Engineering, Suzhou University of Science and Technology, Suzhou 215009, China*
[2]*School of Science, Nanjing University of Science and Technology, Nanjing 210094, China*
[3]*Institute for Automatic Control and Complex Systems (AKS), Faculty of Engineering, University of Duisburg-Essen, Duisburg, Germany*
[4]*College of Electrical Engineering, Zhejiang University, Hangzhou 310027, China*

Correspondence should be addressed to Fuyuan Hu; fuyuanhu@mail.usts.edu.cn and Qing Gao; qing.gao.chance@gmail.com

Received 26 September 2017; Revised 12 December 2017; Accepted 16 January 2018; Published 11 April 2018

Academic Editor: Chengyuan Wang

Graphene sheets are widely applied due to their unique and highly valuable properties, such as energy conservation materials in buildings. In this paper, we investigate the vibration behavior of double layer graphene sheets (DLGSs) in thermal environments which helps probe into the mechanism of energy conservation of graphene sheets in building materials. The nonlocal elastic theory and classical plate theory (CLPT) are used to derive the governing equations. The element-free method is employed to analyze the vibration behaviors of DLGSs embedded in an elastic medium. The accuracy of the solutions in this study is demonstrated by comparison with published results in the literature. Furthermore, a number of numerical results are presented to investigate the effects of various parameters (boundary conditions, nonlocal parameter, aspect ratio, side length, elastic foundation parameter, and temperature) on the frequency of DLGSs.

1. Introduction

In 2004, Novoselov and Geim in [1], physicists at the University of Manchester, successfully stripped off graphene sheets from the graphite. Graphene sheets (GSs) have carbon atomic structure of the monolayer or multilayer atomic thickness. DLGSs in which the interlayer width is 0.34 nm [2] have specific chemical, mechanical, thermal, and electronic properties [3–10] and have been applied as constituent in nanoelectromechanical systems (NEMS) and microelectromechanical systems (MEMS). DLGSs used in these applications generally rest on the elastic medium rather than being suspended. Due to the increasing applications of graphene sheets, understanding the vibration of DLGSs embedded in the elastic media is essential to optimize the design and manufacture in engineering.

Applications of DLGSs depend on clear knowledge of their mechanical behavior. In recent years, world-wide researchers have engaged in the study of GSs using experimental, numerical, and theoretical tools. However, it is of difficulty to carry out experimental research due to the very small dimensions of the nanostructure elements [11]. Thus, theoretical research is becoming increasingly important for studying nanostructures. The theoretical tools can be divided into three categories [12]: atomistic modeling, continuum mechanics (CM), and the hybrid method. Generally, the atomistic modeling consists of classic tight-binding molecular dynamics (TBMD) and molecular dynamics (MD). Mirparizi and Aski [13] studied the interlayer shear effect on vibrational behavior for DLGSs using the MD simulation. Gajbhiye and Singh [14] studied the nonlinear frequency response of SLGSs via the atomistic finite element method

(FEM). The MD simulation is still the most sophisticated and reliable approach which provides deep insight into nanomaterials and their properties. However, MD simulation is limited to the analysis of GSs with few atoms and time scales because of high computational cost. Thus, unlike MD simulations, the CM has a lower computational cost [15] and has been adopted by numerous researchers to deal with nanoscale structures. Therefore, some relatively large nanostructures can be analyzed by this method [16, 17]. The classical continuum approach is however a kind of scale-free theory which cannot account for the small scale effect arising in the nanostructures. Therefore, the mechanical behavior of nanostructures cannot be successfully captured by the classical continuum approach. It behooves us to modify the classical continuum model which can describe precise mechanical behaviors of the nanostructures. Some improved continuum methods such as couple stress theory [18], surface elasticity theory [19], nonlocal theory, and strain gradient theory [20] were used in the simulation of the size-dependent materials. It is found that the nonlocal theory has provided good matching results compared with lattice dynamics. Recent literature indicates that the theory of nonlocal elasticity is being increasingly used [21–23]. Peddieson et al. [24] were the first ones who adopted the nonlocal elasticity theory to analyze the static deformation behavior of Euler-Bernoulli nanobeams. Duan and Wang [25] firstly formulated the nonlocal continuum plate model to study the small scale effect in the bending regarding circular nanoplates. Dastjerdi and Jabbarzadeh [26] studied the multilayer orthotropic circular GSs nonlinear bending using nonlocal elasticity theory. Liew et al. [27] investigated the effect of polymer matrix on the vibration response of GSs. Zhang et al. [12] studied the free vibration behaviors of DLGSs employing nonlocal elasticity theory. Zhang et al. [28] analyzed the vibration of quadrilateral graphene sheets subjected to an in-plane magnet using nonlocal elasticity theory. Pradhan and Phadikar [29] conducted the vibration analysis of double-layered GSs resting on a polymer matrix utilizing the nonlocal continuum mechanics. Malekzadeh et al. [21] investigated the small scale effect on the thermal buckling characteristic of orthotropic arbitrary straight-sided quadrilateral nanoplates embedded in an elastic medium. Asemi et al. [30] presented an axisymmetric buckling analysis of circular SLGS using Eringen's theory. Additionally, Asemi et al. [31] used nonlocal theory of Eringen to simulate postbuckling response of orthotropic SLGS.

Numerical techniques are important for theoretical analysis. Various numerical tools have been utilized to analyze the mechanical behaviors of nanostructure [32, 33]. Ansari et al. [34] proposed a nonlocal FEM model to simulate the vibration behaviors of multilayered GSs based on the Mindlin plate theory. As a numerical technique, the meshless method has been successfully applied in solving engineering problems. Because of its advantage of not relying on elements, it has good adaptability [35–39].

In this work, we study the vibration behavior of DLGSs resting on a Pasternak elastic medium employing the nonlocal theory and established the meshless framework to obtain the solution. The effects of nonlocal parameter, temperature, aspect ratio, side length, stacking types, and foundation parameters on the vibration frequency of DLGSs are examined. Additionally, the accuracy of the solutions in this study is demonstrated through comparison with published results in the literature.

2. Nonlocal Elasticity Theory and Model of Elastic Medium

2.1. Nonlocal Elasticity Theory. Eringen [36] proposed the nonlocal theory through experiment and the theoretical analysis in which the stress depends on the strain of all the points in the domain. Therefore, it can reflect the small scale effect. The most widely applied constitutive relation of the differential form is written as

$$\left[1 - \left(e_0 a\right)^2 \nabla^2\right] \sigma_{ij}(x) = C_{ijkl} \varepsilon_{kl}(x), \tag{1}$$

in which $e_0 a$ is the nonlocal parameter and ∇^2 is the Laplacian operator defined by $\nabla^2 = \partial^2/\partial x^2 + \partial^2/\partial y^2$.

2.2. Model of Elastic Medium. In nanoscale devices, vibration behaviors can be observed, which affect the performance significantly. As mentioned above, graphene based products are usually resting on an elastic medium. In the present study, the Pasternak-type foundation [40] is adopted. Pasternak-type foundation model is modeled with two parameters. The mathematical expressions of Pasternak-type foundation are written as

$$q_{\text{pasternak}} = k_w w - k_g \nabla^2 w, \tag{2}$$

where k_w is the Winker modulus and k_g is the shear modulus.

2.3. Temperature Field Distribution Type. In this paper, the temperature field can be divided into three types as linear, nonlinear, and uniform. The temperature changes along the thickness of the GSs. The temperature change obeys the following law [22]:

$$\Delta T(z) = \left(\frac{z + h/2}{z}\right)^{\varphi} T, \quad \frac{-h}{2} \le z \le \frac{h}{2}, \tag{3}$$

where φ is the temperature distribution coefficient. When $\varphi > 1$, there is a nonlinear temperature distribution along the thickness of the GSs; for $\varphi = 1$ we have a linear temperature distribution, for $\varphi = 0$ the temperature distribution is uniform, and the temperature change is $T = T_b - T_r$, where T_b is the temperature value when the buckling occurs, while T_r is the referent temperature. The thermal load caused by temperature change satisfies the following formulation:

$$\begin{aligned} N_T &= -\frac{\alpha E}{1 - \upsilon} \int_{-h/2}^{h/2} \left(\frac{z + h/2}{z}\right)^{\varphi} T \, dz \\ &= -\frac{\alpha h E}{(1 - \upsilon)(1 + \varphi)} T. \end{aligned} \tag{4}$$

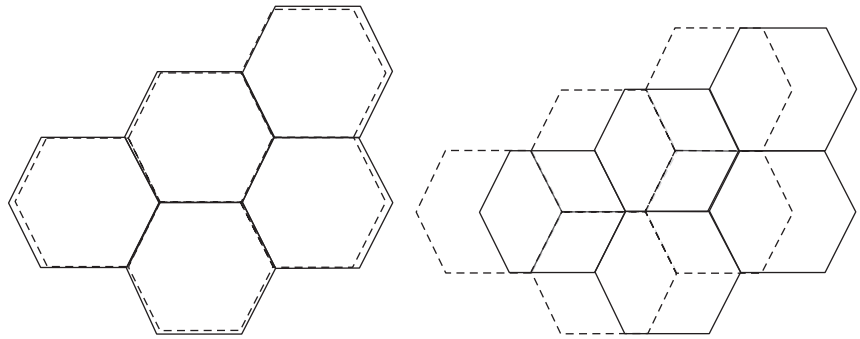

Figure 1: Two stacking types of DLGSs.

3. Theoretical Approach

3.1. The Van der Waals (vdW) Force Expression. In DLGSs, the interaction force between layers is the vdW force which is a nonbonded interaction. By neglecting the nonlinear terms, the vdW's interaction can be expressed as [41]

$$q_{ij} = c_{ij}\left(w_i - w_j\right), \quad i, j = 1, 2 \tag{5}$$

in which c_{ij} represents the vdW coefficient. Generally, DLGSs consist of two types in terms of the relative positions of the upper and lower layers. The one with the upper graphene layer stacking directly on lower layer is called AA-type whereas the other is called AB-type [41]. Figure 1 depicts these two categories of DLGSs. According to [41], the vdW coefficient is

$$\begin{aligned} c_{ij} &= -27.3546\,\text{Gpa/nm} \quad (\text{for AA-type}), \\ c_{ij} &= -146.8247\,\text{Gpa/nm} \quad (\text{for AB-type}). \end{aligned} \tag{6}$$

If there is no special description, the vdW coefficient is taken as AB-type in the following simulations.

3.2. Governing Equations. The DLGSs resting on elastic foundation are demonstrated in Figure 2 in which they are in the thermal condition. The external foundation is modeled as Pasternak-type. L_x and L_y, respectively, denote the length and width of GSs. The thickness of graphene is h. Transverse displacements of the top-GSs and bottom-GSs for the buckling analysis are represented by $w_1(x, y, t)$ and $w_2(x, y, t)$, respectively.

The displacement field of DLGSs according to CLPT can be written as

$$\begin{aligned} u(x, y, z; t) &= \frac{-z\partial w_1(x, y; t)}{\partial x} \\ v(x, y, z; t) &= \frac{-z\partial w_1(x, y; t)}{\partial y} \\ w(x, y, z; t) &= w_1(x, y; t) \end{aligned} \tag{7}$$

in which (u, v, w), respectively, denote the displacements along the axes (x, y, z). w_1 is the displacement along z-axis of a mid-plane material point. According to the strain-displacement relations

$$\varepsilon_{1xx} = \frac{-z\partial^2 w_1(x, y; t)}{\partial x^2} \tag{8}$$

$$\varepsilon_{1yy} = \frac{-z\partial^2 w_1(x, y; t)}{\partial y^2} \tag{9}$$

$$\gamma_{1xy} = \frac{-2z\partial^2 w_1(x, y; t)}{\partial x\partial y} \tag{10}$$

$$\varepsilon_{1zz} = \gamma_{1xz} = \gamma_{1yz} = 0 \tag{11}$$

the constitutive relationship is given by

$$\begin{aligned} &\left[1 - (e_0 a)^2 \nabla^2\right] \begin{Bmatrix} \sigma_{1xx} \\ \sigma_{1yy} \\ \sigma_{1xy} \end{Bmatrix} \\ &= \begin{bmatrix} \dfrac{E}{(1-\upsilon^2)} & \dfrac{\upsilon E}{(1-\upsilon^2)} & 0 \\ \dfrac{\upsilon E}{(1-\upsilon^2)} & \dfrac{E}{(1-\upsilon^2)} & 0 \\ 0 & 0 & G \end{bmatrix} \begin{bmatrix} \varepsilon_{1xx} - \alpha\Delta T \\ \varepsilon_{1yy} - \alpha\Delta T \\ \varepsilon_{1xy} \end{bmatrix}, \end{aligned} \tag{12}$$

where $G = E/2(1 + \upsilon)$.

According to (10), the nonlocal moments can be written as

$$\begin{aligned} &\left[1 - (e_0 a)^2 \nabla^2\right] M_{1xx} \\ &= -D\left(\frac{\partial^2 w_1(x, y; t)}{\partial x^2} + \frac{\upsilon\partial^2 w_1(x, y; t)}{\partial y^2}\right), \end{aligned} \tag{13}$$

$$\begin{aligned} &\left[1 - (e_0 a)^2 \nabla^2\right] M_{1yy} \\ &= -D\left(\frac{\partial^2 w_1(x, y; t)}{\partial y^2} + \frac{\upsilon\partial^2 w_1(x, y; t)}{\partial x^2}\right), \end{aligned} \tag{14}$$

$$\left[1 - (e_0 a)^2 \nabla^2\right] M_{1xy} = \frac{-D(1-\upsilon)\partial^2 w_1(x, y; t)}{\partial x\partial y}, \tag{15}$$

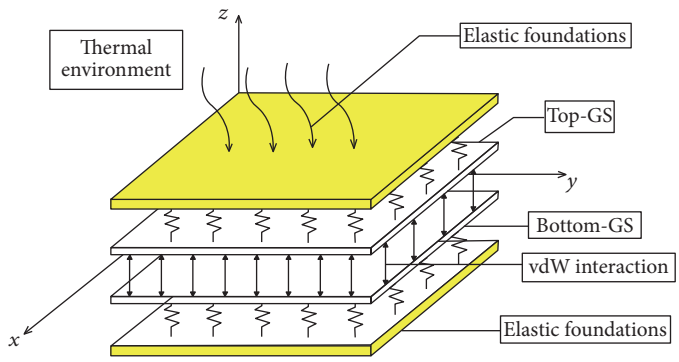

Figure 2: DLGSs resting on Pasternak-type elastic foundation under thermal environment.

where $(M_{1xx}, M_{1yy}, M_{xy}) = \int(\sigma_{1xx}, \sigma_{1yy}, \sigma_{1xy})z\,dz$. D is the bending stiffness of the plate and $D = Eh^3/12(1-\upsilon^2)$.

With the principle of virtual work, the equilibrium equation can be derived as

$$\begin{aligned} &-M_{1xx,xx} - M_{1yy,yy} - 2M_{1xy,xy} - q_{12} + k_w w_1 \\ &\quad - k_g\nabla^2 w_1 - N_T\nabla^2 w_1 - I_2\left(\ddot{w}_{1,xx} + \ddot{w}_{1,yy}\right) \\ &\quad + I_0\ddot{w}_1 = 0. \end{aligned} \tag{16}$$

From (11)–(13), we can get

$$\begin{aligned} &-D\nabla^4 w_1 \\ &= \left[1 - (e_0a)^2\nabla^2\right]\left(M_{1xx,xx} + M_{1yy,yy} + 2M_{1xy,xy}\right). \end{aligned} \tag{17}$$

Substituting (17) into (16), the governing equation can be written as

$$\begin{aligned} &D\nabla^4 w_1 + \left[1 - (e_0a)^2\nabla^2\right]\left[-q_{12} + k_w w_1 - k_g\nabla^2 w_1\right. \\ &\quad \left. - N_T\nabla^2 w_1 - I_2\left(\ddot{w}_{1,xx} + \ddot{w}_{1,yy}\right) + I_0\ddot{w}_1\right]. \end{aligned} \tag{18}$$

Similarly, we can obtain the governing equation of bottom-GSs

$$\begin{aligned} &D\nabla^4 w_2 + \left[1 - (e_0a)^2\nabla^2\right]\left[-q_{21} + k_w w_2 - k_g\nabla^2 w_2\right. \\ &\quad \left. - N_T\nabla^2 w_2 - I_2\left(\ddot{w}_{2,xx} + \ddot{w}_{2,yy}\right) + I_0\ddot{w}_2\right]. \end{aligned} \tag{19}$$

4. Discretized System Equations

4.1. Weak Form. In order to get the weak form, the equilibrium equation is multiplied by the virtual displacement δw. Therefore, we obtain

$$\begin{aligned} &\int_\Omega \delta w_1\left(D\nabla^4 w_1 + \left[1 - (e_0a)^2\nabla^2\right]\left(-q_{12} + k_w w_1\right.\right. \\ &\quad - N_T\nabla^2 w_1 - k_g\nabla^2 w_1 + I_0\ddot{w}_1 \\ &\quad \left.\left. - I_2\left(\ddot{w}_{1,xxtt} + \ddot{w}_{1,yytt}\right)\right)\right)dx\,dy = 0. \end{aligned} \tag{20}$$

Equation (20) can be integrated by parts as

$$\begin{aligned} &D\int_\Omega\left(w_{1,xx}\delta w_{1,xx} + w_{1,yy}\delta w_{1,yy}\right. \\ &\quad \left. + 2w_{1,xy}\delta w_{1,xy}\right)dx\,dy - c\int_\Omega\left(w_1\delta w_1\right. \\ &\quad \left. - w_2\delta w_1\right)\int_\Omega\left(w_{1,xx}\delta w_{1,xx} + w_{1,yy}\delta w_{1,yy}\right. \\ &\quad \left. + 2w_{1,xy}\delta w_{1,xy}\right)dx\,dy \\ &\quad + k_w\int_\Omega w_1\delta w_1\int_\Omega\left(w_{1,xx}\delta w_{1,xx} + w_{1,yy}\delta w_{1,yy}\right. \\ &\quad \left. + 2w_{1,xy}\delta w_{1,xy}\right)dx\,dy + (e_0a)^2 \\ &\quad \cdot k_w\int_\Omega\left(w_{1,x}\delta w_{1,x} + w_{1,y}\delta w_{1,y}\right)\int_\Omega\left(w_{1,xx}\delta w_{1,xx}\right. \\ &\quad \left. + w_{1,yy}\delta w_{1,yy} + 2w_{1,xy}\delta w_{1,xy}\right)dx\,dy \\ &\quad + N_T\int_\Omega w_{1,x}\delta w_{1,x}\int_\Omega\left(w_{1,xx}\delta w_{1,xx} + w_{1,yy}\delta w_{1,yy}\right. \\ &\quad \left. + 2w_{1,xy}\delta w_{1,xy}\right)dx\,dy - c(e_0a)^2 \\ &\quad \cdot\int_\Omega\left(w_{1,x}\delta w_{1,x} + w_{1,y}\delta w_{1,y}\right)\int_\Omega\left(w_{1,xx}\delta w_{1,xx}\right. \\ &\quad \left. + w_{1,yy}\delta w_{1,yy} + 2w_{1,xy}\delta w_{1,xy}\right)dx\,dy \\ &\quad + (e_0a)^2 N_T\int_\Omega\left(w_{1,xx}\delta w_{1,xx} + w_{1,xy}\delta w_{1,xy}\right) \\ &\quad \cdot\int_\Omega\left(w_{1,xx}\delta w_{1,xx} + w_{1,yy}\delta w_{1,yy}\right. \\ &\quad \left. + 2w_{1,xy}\delta w_{1,xy}\right)dx\,dy + c(e_0a)^2 \\ &\quad \cdot\int_\Omega\left(w_{2,x}\delta w_{1,x} + w_{2,y}\delta w_{1,y}\right)\int_\Omega\left(w_{1,xx}\delta w_{1,xx}\right. \\ &\quad \left. + w_{1,yy}\delta w_{1,yy} + 2w_{1,xy}\delta w_{1,xy}\right)dx\,dy \end{aligned}$$

$$
\begin{aligned}
&+ k_g \int_\Omega \left(w_{1,x}\delta w_{1,x} + w_{1,y}\delta w_{1,y}\right) \int_\Omega \left(w_{1,xx}\delta w_{1,xx}\right.\\
&\left.+ w_{1,yy}\delta w_{1,yy} + 2w_{1,xy}\delta w_{1,xy}\right) dx\, dy\\
&+ (e_0 a)^2 \int_\Omega I_0 \left(\delta w_{1,x} w_{1,xtt} + \delta w_{1,y} w_{1,ytt}\right)\\
&+ I_2 \left(\delta w_{1,xx} w_{1,xxtt} + 2\delta w_{1,xy} w_{1,xytt}\right.\\
&\left.+ \delta w_{1,yy} w_{1,yytt}\right) \int_\Omega \left(w_{1,xx}\delta w_{1,xx} + w_{1,yy}\delta w_{1,yy}\right.\\
&\left.+ 2w_{1,xy}\delta w_{1,xy}\right) dx\, dy + (e_0 a)^2\\
&\cdot N_T \int_\Omega \left(w_{1,xy}\delta w_{1,xy} + w_{1,yy}\delta w_{1,yy}\right)\\
&\cdot \int_\Omega \left(w_{1,xx}\delta w_{1,xx} + w_{1,yy}\delta w_{1,yy}\right.\\
&\left.+ 2w_{1,xy}\delta w_{1,xy}\right) dx\, dy\\
&+ N_T \int_\Omega w_{1,y}\delta w_{1,y} \int_\Omega \left(w_{1,xx}\delta w_{1,xx} + w_{1,yy}\delta w_{1,yy}\right.\\
&\left.+ 2w_{1,xy}\delta w_{1,xy}\right) dx\, dy + k_g (e_0 a)^2\\
&\cdot \int_\Omega \left(w_{1,xx}\delta w_{1,xx} + w_{1,yy}\delta w_{1,yy} + 2w_{1,xy}\delta w_{1,xy}\right)\\
&\cdot \int_\Omega \left(w_{1,xx}\delta w_{1,xx} + w_{1,yy}\delta w_{1,yy}\right.\\
&\left.+ 2w_{1,xy}\delta w_{1,xy}\right) dx\, dy\\
&+ \int_\Omega \left[I_0 \delta w_1 w_{1,tt} + I_2 \left(\delta w_{1,x} w_{1,xtt} + \delta w_{1,y} w_{1,ytt}\right)\right]\\
&\cdot \int_\Omega \left(w_{1,xx}\delta w_{1,xx} + w_{1,yy}\delta w_{1,yy}\right.\\
&\left.+ 2w_{1,xy}\delta w_{1,xy}\right) dx\, dy - (e_0 a)^2\\
&\cdot k_w \int_\Gamma \left(w_{1,x}\delta w_1 n_x - w_{1,y}\delta w_1 n_y\right) ds\\
&- N_T \int_\Gamma w_{1,x}\delta w_1 n_x ds + N_T \int_\Gamma w_{1,y}\delta w_1 n_y ds\\
&+ (e_0 a)^2 N_T \int_\Gamma \left(w_{1,xxx}\delta w_1 n_x - w_{1,xx}\delta w_{1,x} n_x\right.\\
&\left.+ w_{1,xyy}\delta w_1 n_x + w_{1,xy}\delta w_{1,x} n_y\right) ds + (e_0 a)^2\\
&\cdot N_T \int_\Gamma \left(w_{1,xyy}\delta w_1 n_x + w_{1,xy}\delta w_{1,x} n_y\right.\\
&\left.- w_{1,yyy}\delta w_1 n_y + w_{1,yy}\delta w_{1,y} n_y\right) ds\\
&+ k_g (e_0 a)^2 \int_\Gamma \left(w_{1,xxx}\delta w_1 n_x - w_{1,xx}\delta w_{1,x} n_x\right.\\
&\left.- w_{1,yyy}\delta w_1 n_y + w_{1,yy}\delta w_{1,y} n_y + 2w_{1,xyy}\delta w_1 n_x\right.\\
&\left.+ 2w_{1,xy}\delta w_{1,x} n_y\right) ds + D \int_\Gamma \left(w_{1,xxx}\delta w_1 n_x\right.\\
&\left.- w_{1,xx}\delta w_{1,x} n_x - w_{1,yyy}\delta w_1 n_y + w_{1,yy}\delta w_{1,y} n_y\right.\\
&\left.+ 2w_{1,xyy}\delta w_1 n_x + 2w_{1,xy}\delta w_{1,x} n_y\right) ds\\
&+ c (e_0 a)^2 \int_\Gamma \left(w_{1,y}\delta w_1 n_y - w_{1,x}\delta w_1 n_x\right.\\
&\left.+ w_{2,x}\delta w_1 n_x - w_{2,y}\delta w_1 n_y\right) ds\\
&+ k_g \int_\Gamma \left(w_{1,y}\delta w_1 n_y - w_{1,x}\delta w_1 n_x\right) ds - (e_0 a)^2\\
&\cdot I_0 \int_\Gamma \left(w_{1,xtt}\delta w_1 n_x - w_{1,ytt}\delta w_1 n_y\right) ds\\
&\cdot I_2 \int_\Gamma \left(w_{1,ytt}\delta w_1 n_y - w_{1,xtt}\delta w_1 n_y\right) ds + (e_0 a)^2\\
&\cdot I_2 \int_\Gamma \left(w_{1,xxxtt}\delta w_1 n_x - w_{1,xxtt}\delta w_{1,x} n_x\right.\\
&\left.- w_{1,yyytt}\delta w_1 n_y + w_{1,yytt}\delta w_{1,y} n_y\right.\\
&\left.+ 2w_{1,xyytt}\delta w_1 n_x + 2w_{1,xytt}\delta w_{1,x} n_y\right) ds = 0.
\end{aligned}
\tag{21}
$$

Equation (19) has the following weak form:

$$
\begin{aligned}
&\int_\Omega \delta w_2 \left(D\nabla^4 w_2 + \left[1 - (e_0 a)^2 \nabla^2\right]\left(-q_{21} + k_w w_2\right.\right.\\
&\left.\left.- N_T \nabla^2 w_2 - k_g \nabla^2 w_2 + I_0 \ddot{w}_2\right.\right.\\
&\left.\left.- I_2 \left(\ddot{w}_{2,xxtt} + \ddot{w}_{2,yytt}\right)\right)\right) dx\, dy = 0
\end{aligned}
\tag{22}
$$

Equation (22) can be dealt with similarly.

4.2. Element-Free Discretization Technique. Using M values of the scattered particles $(\mathbf{x}_1, \mathbf{x}_2, \ldots, \mathbf{x}_M)$ to express the displacement field of SLGSs based on the kernel particle Ritz method [42] results in

$$
\begin{bmatrix} w_1 \\ w_2 \end{bmatrix} = \sum_{I=1}^{M} \psi_I (x, y) \begin{bmatrix} w_{1I} \\ w_{2I} \end{bmatrix}. \tag{23}
$$

where m is the number of nodes. w_I and ψ_I, respectively, denote the displacement value and the shape function regarding node I. We write the shape function as

$$
\psi_I = C (\mathbf{x}; \mathbf{x} - \mathbf{x}_\mathbf{I}) \Phi (\mathbf{x} - \mathbf{x}_\mathbf{I}). \tag{24}
$$

Herein, $C(\mathbf{x};\mathbf{x}-\mathbf{x_I})$ is the coefficient function and $\Phi(\mathbf{x};\mathbf{x}-\mathbf{x_I})$ represents the kernel function. $C(\mathbf{x};\mathbf{x}-\mathbf{x_I})$ can be expressed as

$$\begin{aligned} C(\mathbf{x};\mathbf{x}-\mathbf{x_I}) &= \mathbf{H}^{\mathrm{T}}(\mathbf{x}-\mathbf{x_I})\,\mathbf{B}(\mathbf{x}),\\ \mathbf{H}^{T}(\mathbf{x}-\mathbf{x_I}) &= \left[1, x-x_I, y-y_I, (x-x_I)(y-y_I),\right.\\ &\quad \left.(x-x_I)^2, (y-y_I)^2\right]^{T},\\ \mathbf{B}(\mathbf{x}) &= \left[k_0(x,y), k_1(x,y), k_2(x,y), k_3(x,y),\right.\\ &\quad \left.k_4(x,y), k_5(x,y)\right]^{T}, \end{aligned} \tag{25}$$

where $\mathbf{H}$ denotes the vector of the quadratic basis and $\mathbf{B}$ represents the function of $\mathbf{x}$. Thus, we have

$$\Psi_I(\mathbf{x};\mathbf{x}-\mathbf{x_I}) = \mathbf{B}^{T}(\mathbf{x})\,\mathbf{H}(\mathbf{x}-\mathbf{x_I})\,\mathbf{\Phi}(\mathbf{x}-\mathbf{x_I}), \tag{26}$$

satisfying the shape function to reproduction conditions resulting in

$$\sum_{I=1}^{M}\Psi_I(x)\,x_I^{p}y_I^{q} \quad \text{for } p+q=0,1,2. \tag{27}$$

Coefficient $\mathbf{B}(\mathbf{x})$ has the following form:

$$\mathbf{B}(\mathbf{x}) = \mathbf{M}^{-1}(\mathbf{x})\,\mathbf{H}(\mathbf{0}), \tag{28}$$

where

$$\begin{aligned} \mathbf{M}(\mathbf{x}) &= \sum_{I=1}^{M}\mathbf{H}(\mathbf{x}-\mathbf{x_I})\,\mathbf{\Phi}(\mathbf{x}-\mathbf{x_I}),\\ \mathbf{H}(\mathbf{0}) &= [1,0,0,0,0,0]^{T}. \end{aligned} \tag{29}$$

We have the kernel function

$$\Phi(\mathbf{x}-\mathbf{x_I}) = \Phi(x;x_I)\cdot\Phi(y;y_I), \tag{30}$$

where

$$\Phi(x;x_I) = \phi\left(\frac{|x-x_I|}{a_I}\right). \tag{31}$$

The cubic spline function is used in the present study

$$\phi(s_1) = \begin{cases} \dfrac{2}{3} - 4s_1^2 + 4s_1^3 & \text{for } 0 \le s_1 \le \dfrac{1}{2}\\ \dfrac{4}{3} - 4s_1 + 4s_1^2 - \dfrac{4}{3}s_1^3 & \text{for } \dfrac{1}{2} \le s_1 \le 1\\ 0 & \text{otherwise,} \end{cases} \tag{32}$$

where $s_1 = |x-x_I|/a_I$, $a_I = a(x_I)$ are the dilation parameters. a_I can be expressed as $a_I = d_{\max}c_I$, where $d_{\max}$ denotes the scaling factor ranging between 2 and 4. To ensure that the support area contains numerous enough nodes to prevent the matrix $\mathbf{M}$ from singularity, the factor should be selected appropriately. c_I denotes the larger distances.

4.3. Discrete System Equations. Where $N_T = -T(\alpha hE)/[(1-\upsilon)(1+\varphi)]$ and substituting (21) into (16), the discrete equation can be expressed as

$$\mathbf{M}_{11}\ddot{\mathbf{w}}_1 + (\mathbf{k}_{11}+\mathbf{k}_T)\,\mathbf{w}_1 + \mathbf{k}_{12}\mathbf{w}_2 = \mathbf{0}, \tag{33}$$

where

$$\mathbf{M}_{11} = \mathbf{M}_{11}^{l} + \mathbf{M}_{11}^{nl}, \tag{34}$$

$$\mathbf{M}_{11}^{l} = \int_{\Omega}\left(I_0\psi_I\psi_J + I_2\left[N_1^I\right]^{T}\left[N_1^J\right]\right)d\Omega, \tag{35}$$

$$\begin{aligned} &\mathbf{M}_{11}^{nl}\\ &\quad = \int_{\Omega}(e_0a)^2\left(I_0\left[N_1^I\right]^{T}\left[N_1^J\right] + \left[N_2^I\right]^{T}\mathbf{I}\left[N_2^J\right]\right)d\Omega, \end{aligned} \tag{36}$$

$$\mathbf{k}_{11} = \mathbf{k}_{11}^{l} + \mathbf{k}_{11}^{nl} + \mathbf{k}_{\text{medium}}, \tag{37}$$

$$\mathbf{k}_{11}^{l} = \int_{\Omega}\left[N_2^I\right]^{T}\mathbf{L}_D\left[N_2^J\right] - c\psi_I\psi_J d\Omega, \tag{38}$$

$$\mathbf{k}_{11}^{nl} = \int_{\Omega} -c(e_0a)^2\left[N_1^I\right]^{T}\left[N_1^J\right]d\Omega, \tag{39}$$

$$\mathbf{k}_{\text{medium}} = \int_{\Omega}\left[N_4^I\right]^{T}\mathbf{L}_G\left[N_4^J\right] + \left[N_3^I\right]^{T}\mathbf{L}_w\left[N_3^J\right]d\Omega, \tag{40}$$

$$\mathbf{k}_{12} = \mathbf{k}_{12}^{l} + \mathbf{k}_{12}^{nl}, \tag{41}$$

$$\mathbf{k}_{12}^{l} = \int_{\Omega} c\psi_I\psi_J d\Omega, \tag{42}$$

$$\mathbf{k}_{12}^{nl} = \int_{\Omega} c(e_0a)^2\left[N_1^I\right]^{T}\left[N_1^J\right]d\Omega, \tag{43}$$

$$\mathbf{k}_T = \int_{\Omega}\left[N_4^I\right]^{T}L_T\left[N_4^J\right]d\Omega. \tag{44}$$

Similarly, we can obtain

$$\mathbf{M}_{22}\ddot{\mathbf{w}}_2 + \mathbf{k}_{21}\mathbf{w}_1 + (\mathbf{k}_{22}+\mathbf{k}_T)\,\mathbf{w}_2 = \mathbf{0} \tag{45}$$

$$\mathbf{M}_{11} = \mathbf{M}_{22}, \tag{46}$$

$$\mathbf{k}_{21} = \mathbf{k}_{21}^{l} + \mathbf{k}_{21}^{nl}, \tag{47}$$

$$\mathbf{k}_{21}^{l} = \int_{\Omega} c\psi_I\psi_J d\Omega, \tag{48}$$

$$\mathbf{k}_{21}^{nl} = \int_{\Omega} c(e_0a)^2\left[N_1^I\right]^{T}\left[N_1^J\right]d\Omega, \tag{49}$$

$$\mathbf{k}_{22} = \mathbf{k}_{22}^{l} + \mathbf{k}_{22}^{nl} + \mathbf{k}_{\text{medium}}, \tag{50}$$

$$\mathbf{k}_{22}^{l} = \int_{\Omega}\left[N_2^I\right]^{T}\mathbf{L}_D\left[N_2^J\right] - c\psi_I\psi_J d\Omega, \tag{51}$$

$$\mathbf{k}_{22}^{nl} = \int_{\Omega} -c(e_0a)^2\left[N_1^I\right]^{T}\left[N_1^J\right]d\Omega, \tag{52}$$

$$\mathbf{L}_T = \frac{-\alpha h E T}{(1-\upsilon)(1+\varphi)} \begin{bmatrix} 1 & 0 & 0 & 0 & 0 \\ 0 & (e_0 a)^2 & & & \\ & & 2(e_0 a)^2 & & \\ & & & 1 & \\ & & & & (e_0 a)^2 \end{bmatrix}, \quad (53)$$

$$\mathbf{I} = \begin{bmatrix} I_2 & 0 & 0 \\ 0 & 2I_2 & 0 \\ 0 & 0 & I_2 \end{bmatrix},$$

$$\mathbf{L}_D = \begin{bmatrix} D & 0 & 0 \\ 0 & 2D & 0 \\ 0 & 0 & D \end{bmatrix}, \quad (54)$$

$$\mathbf{L}_w = \begin{bmatrix} k_w & 0 & 0 \\ 0 & (e_0 a)^2 k_w & 0 \\ 0 & 0 & (e_0 a)^2 k_w \end{bmatrix},$$

$$\mathbf{L}_G = \begin{bmatrix} k_g & 0 & 0 & 0 & 0 \\ 0 & k_g (e_0 a)^2 & 0 & 0 & 0 \\ 0 & 0 & 2k_g (e_0 a)^2 & 0 & 0 \\ 0 & 0 & 0 & k_g & 0 \\ 0 & 0 & 0 & 0 & k_g (e_0 a)^2 \end{bmatrix}, \quad (55)$$

$$\left[N_1^I\right] = \begin{bmatrix} \psi_{I,x} \\ \psi_{I,y} \end{bmatrix},$$

$$\left[N_2^I\right] = \begin{bmatrix} \psi_{I,xx} \\ \psi_{I,xy} \\ \psi_{I,yy} \end{bmatrix},$$

$$\left[N_3^I\right] = \begin{bmatrix} \psi_I \\ \psi_{I,x} \\ \psi_{I,y} \end{bmatrix}, \quad (56)$$

$$\left[N_4^I\right] = \begin{bmatrix} \psi_{I,x} \\ \psi_{I,xx} \\ \psi_{I,xy} \\ \psi_{I,y} \\ \psi_{I,yy} \end{bmatrix}.$$

We rearrange matrix equations (31) and (43) as

$$\begin{bmatrix} \mathbf{M}_{11} & \mathbf{0} \\ \mathbf{0} & \mathbf{M}_{22} \end{bmatrix} \begin{bmatrix} \ddot{\mathbf{w}}_1 \\ \ddot{\mathbf{w}}_2 \end{bmatrix} + \begin{bmatrix} \mathbf{k}_{11} + \mathbf{k}_T & \mathbf{k}_{12} \\ \mathbf{k}_{21} & \mathbf{k}_{22} + \mathbf{k}_T \end{bmatrix} = \mathbf{0}. \quad (57)$$

Table 1: Mechanical properties.

E	h	ρ	υ
1.06 TPa	0.34 nm	2250 Kg/m^3	0.25

We assume that

$$\begin{bmatrix} \mathbf{w}_1 \\ \mathbf{w}_2 \end{bmatrix} = \begin{bmatrix} \overline{\mathbf{w}}_1 \\ \overline{\mathbf{w}}_2 \end{bmatrix} e^{i\omega t}. \quad (58)$$

We rewrite (55) as

$$\left(-\omega^2 \begin{bmatrix} \mathbf{M}_{11} & \mathbf{0} \\ \mathbf{0} & \mathbf{M}_{22} \end{bmatrix} + \begin{bmatrix} \mathbf{k}_{11} + \mathbf{k}_T & \mathbf{k}_{12} \\ \mathbf{k}_{21} & \mathbf{k}_{22} + \mathbf{k}_T \end{bmatrix}\right) \begin{bmatrix} \overline{\mathbf{w}}_1 \\ \overline{\mathbf{w}}_2 \end{bmatrix} = \mathbf{0}. \quad (59)$$

By solving eigenvalue problem of (57), the buckling properties of DLCGSs can be presented.

5. Numerical Simulations, Results, and Discussion

In this paper, the nonlocal elastic theory and element-free method are developed for the thermal vibration behavior of DLGSs. The mechanical properties of GSs are shown in Table 1. To verify the effectiveness of the present study, the comparison of the results is given for circular nature frequency for DLGs with the side length of 10 nm for all edges simply supported by the result obtained by [43]. $\omega^i_{(m,n)}$ in this paper represents the ith interlayer vibration mode frequency. From Table 2, the results of the present study agree well with those of He et al. [43].

Firstly, the influence of the side length and the mode (n, m) on the circular natural frequency of the square DLGSs under SSSS boundary condition is plotted in Figure 3. It can be studied that, for all of the first vibration mode, the circular frequencies decrease with the increasing side length whereas, for the second vibration mode, the circular frequencies are not affected by the side length.

Secondly, we conduct a case study on the square DLGSs with 10 nm width to demonstrate the influence of nonlocal parameter on the circular natural frequency. From Figure 4, we also can observe that, for all of the first vibration mode, the circular frequencies decrease with the increasing nonlocal parameter. However, for the second vibration mode, the circular natural frequencies are not influenced by the nonlocal parameters.

Then, in Figure 5, the influence of the aspect ratio on the frequency of DLGSs with the length of 10 nm under various boundary conditions is considered. It can be seen in Figure 5 that, under various boundary conditions, all the first vibration mode circular natural frequencies decrease as the aspect ratio increases. We also can study that, under the same condition, the first interlayer circular natural frequency under CCCC boundary condition is higher than the other boundary condition. However, the second interlayer circular

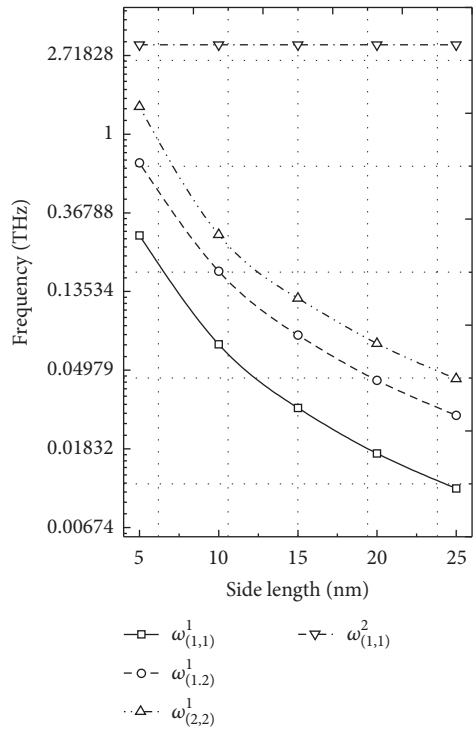

FIGURE 3: Frequency response with the side length for square DLGSs ($T = 0$, $k_g = k_w = 0$, SSSS, $e_0a = 0$).

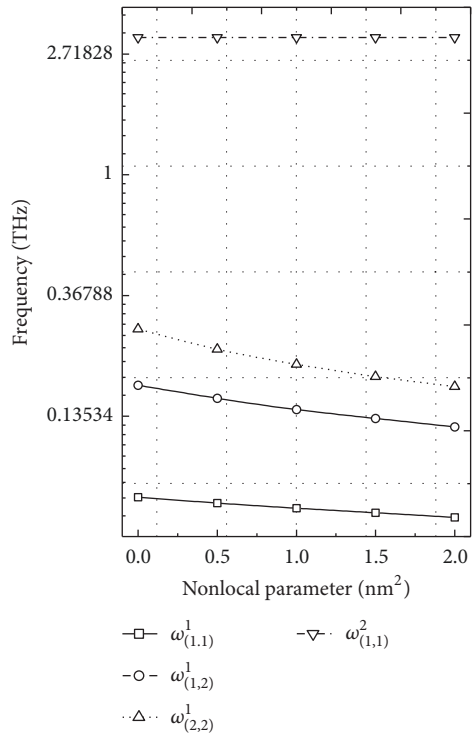

FIGURE 4: Variation of frequency with the nonlocal parameter for square DLGSs ($T = 0$, $k_g = k_w = 0$, SSSS, $L_b = 10\,\text{nm}$).

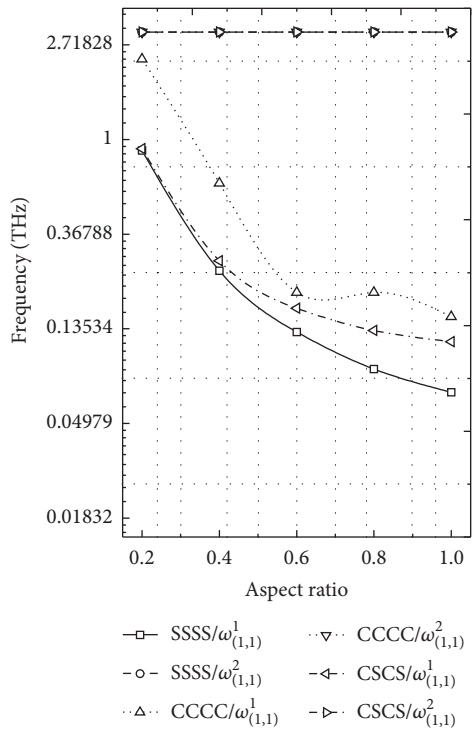

Figure 5: Frequency response with the aspect ratio for DLGSs ($T = 0$, $k_g = k_w = 0$, $L_b = 10$ nm, $e_0 a = 0$).

Table 2: Comparison of the present study with the published ones for square DLGSs with width $b = 10$ nm.

ω (THz)	$\omega^1_{(1,1)}$	$\omega^1_{(1,2)}$	$\omega^1_{(2,1)}$	$\omega^1_{(2,2)}$	$\omega^2_{(1,1)}$	$\omega^2_{(1,2)}$	$\omega^2_{(2,2)}$
He et al.	0.069	0.173	0.173	0.276	2.683	2.688	2.697
Present	0.0692	0.175	0.175	0.2787	2.680	2.684	2.693

natural frequencies under various boundary conditions are not affected by the aspect ratio and the frequencies are the same.

The influence of stacking types of DLGSs on the vibration is also studied. Figure 6 shows the frequency change with the side length under various boundary conditions and two stacking types of DLGSs. Figure 6 indicates that the first interlayer mode circular natural frequency is not affected by the stacking types of DLGSs. However, for second interlayer mode, the circular natural frequency for the AA stacking types is smaller than the AB stacking types.

To study the effects of Pasternak elastic foundation on the interlayer mode circular natural frequency of DLGSs, a case is simulated on square DLGSs with side length of 10 nm under various boundary conditions. The nondimensional Winker modulus parameter $\overline{k}_W$ and shear modulus parameter $\overline{k}_G$ are adopted. The nondimensional parameters are defined as

$$\overline{k}_W = \frac{k_w L_x^4}{D}, \qquad \overline{k}_G = \frac{k_g L_x^2}{D}. \tag{60}$$

As shown in Figure 7, the Winker modulus parameter $\overline{k}_W = 0$. Figure 7 indicates that, for the first vibration mode, the circular frequencies increase with the increasing of $\overline{k}_G$. The first natural frequency under CCCC boundary condition is larger than that under other boundary conditions. In contrast, the second natural frequency is not affected by the shear modulus parameter. Figure 8 shows the relationship between the interlayer circular natural frequency and Winker modulus parameter. It is evident that, for the first mode, the natural frequencies increase with the increasing of Winker modulus parameter. However, for the second mode, the circular natural frequency is not influenced by the Winker modulus parameter.

Finally, to comprehensively understand the effect of the temperature and temperature distribution coefficient on the interlayer mode circular natural frequency, we simulate the vibration behavior of square DLGSs with 10 nm width under SSSS boundary condition. Figure 9 presents the frequency responses under low temperature environment; as shown in Figure 9, under low temperature environment, the interlayer mode circular natural frequency is not affected by the temperature and temperature distribution types. However, as is evident from Figure 10, under high temperature environment, the first interlayer mode circular natural frequency

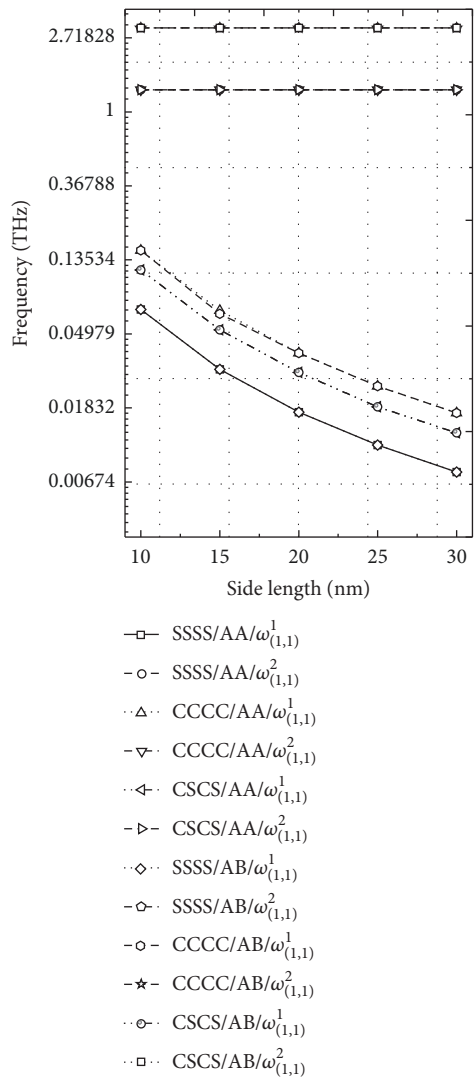

Figure 6: Frequency response with the stacking types for square DLGSs ($T = 0$, $k_g = k_w = 0$, $e_0 a = 0$).

decreases with increasing of the temperature under various temperature distribution types. However, for the second mode, the natural frequency is not affected by either the temperature or the temperature distribution types.

6. Conclusion

In this paper, the nonlocal elasticity theory and element-free method are utilized to reveal the vibration properties of DLGDs resting on a Winker's elastic medium in thermal environment. Influence of side length, nonlocal parameters, boundary conditions, elastic medium parameter, stacking types of graphene, aspect ratio, and temperature distribution types on the interlayer mode circular natural frequency is examined. The results reveal that, for the first mode, the natural frequency is related to the nonlocal parameter, side length, boundary condition, elastic medium parameter, and aspect ratio, but is unrelated to the vdW force. On the contrary, for the second mode, the natural frequency is related to the vdW force, but is not affected by the side length, boundary condition, nonlocal parameter, aspect ratio, elastic medium parameter, and temperature distribution types.

Conflicts of Interest

The authors declare that they have no conflicts of interest.

Acknowledgments

This work is supported by National Natural Science Foundation of China under Grants nos. 71771161, 61472267, 51375323, 61503335, and 71271119, Fundamental Research Funds for the Central Universities under Grant no. 30917011339, Natural Science Foundation of Jiangsu Province under Grant no. BK20170820, Jiangsu Provincial Department of Housing and Urban-Rural Development under Grant no. 2017ZD253,

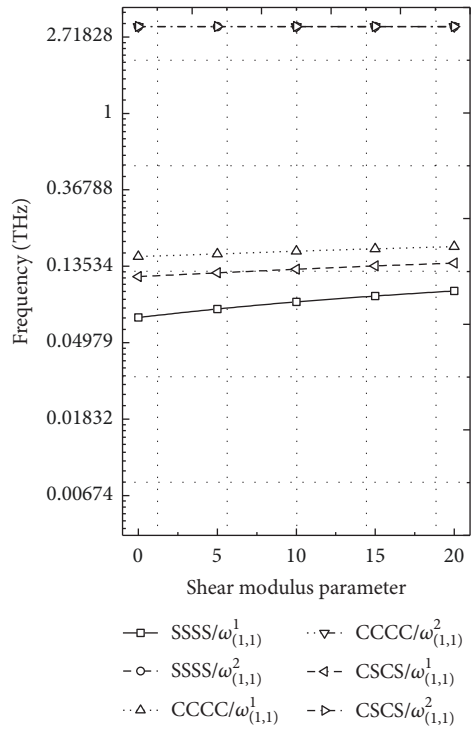

Figure 7: Variation of frequency with the shear modulus parameter for square DLGSs ($T = 0$, $k_w = 0$, $L_b = 10\,\text{nm}$, $e_0a = 0$).

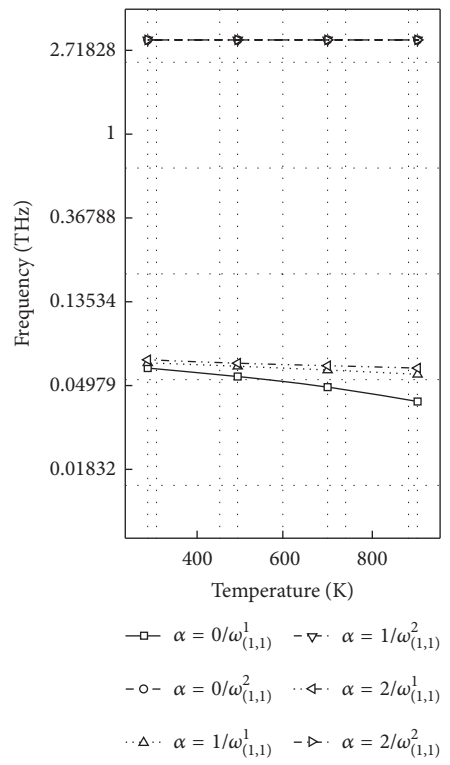

Figure 8: Variation of frequency with the Winker modulus parameter for square DLGSs ($T = 0$, $k_g = 0$, $L_b = 10\,\text{nm}$, $e_0a = 0$).

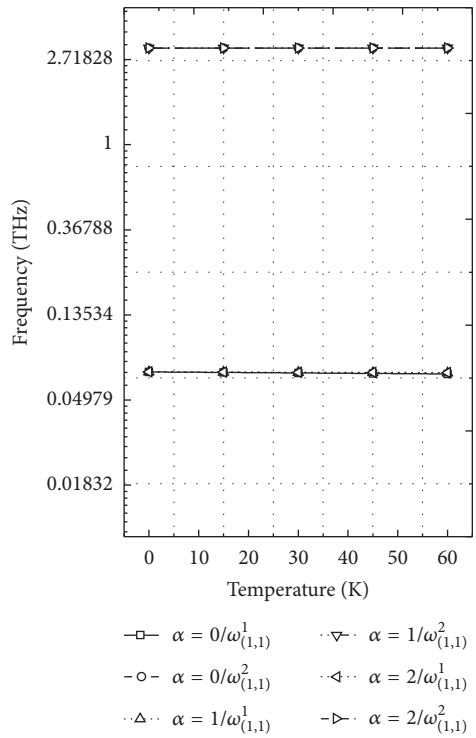

Figure 9: Variation of frequencies with the low temperature for square DLGSs ($k_w = k_g = 0$, $L_b = 10\,\text{nm}$, $e_0a = 0$, SSSS).

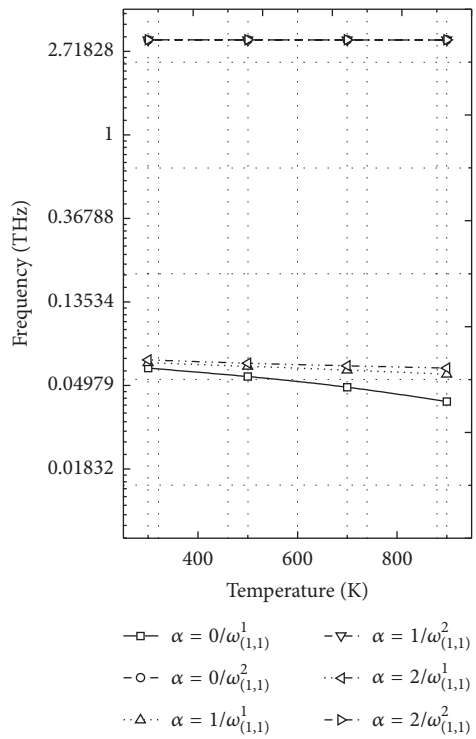

Figure 10: Frequency change with the high temperature for square DLGSs ($k_w = k_g = 0$, $L_b = 10\,\text{nm}$, $e_0a = 0$, SSSS).

Alexander von Humboldt Foundation of Germany, and Social Development Project of Jiangsu Provincial under Grant no. BE2017663.

References

[1] K. S. Novoselov, A. K. Geim, S. V. Morozov et al., "Electric field in atomically thin carbon films," *Science*, vol. 306, no. 5696, pp. 666–669, 2004.

[2] A. Sakhaee-Pour, M. T. Ahmadian, and A. Vafai, "Potential application of single-layered graphene sheet as strain sensor," *Solid State Communications*, vol. 147, no. 7-8, pp. 336–340, 2008.

[3] B. G. Demczyk, Y. M. Wang, J. Cumings et al., "Direct mechanical measurement of the tensile strength and elastic modulus of multiwalled carbon nanotubes," *Materials Science and Engineering: A Structural Materials: Properties, Microstructure and Processing*, vol. 334, no. 1-2, pp. 173–178, 2002.

[4] C. Lee, X. Wei, J. W. Kysar, and J. Hone, "Measurement of the elastic properties and intrinsic strength of monolayer graphene," *Science*, vol. 321, no. 5887, pp. 385–388, 2008.

[5] A. A. Balandin, "Thermal properties of graphene and nanostructured carbon materials," *Nature Materials*, vol. 10, no. 8, pp. 569–581, 2011.

[6] J. S. Bunch, A. M. Van Der Zande, S. S. Verbridge et al., "Electromechanical resonators from graphene sheets," *Science*, vol. 315, no. 5811, pp. 490–493, 2007.

[7] F. Scarpa, S. Adhikari, and A. S. Phani, "Effective elastic mechanical properties of single layer graphene sheets," *Nanotechnology*, vol. 20, no. 6, Article ID 065709, 2009.

[8] Y. Shao, J. Wang, H. Wu, J. Liu, I. A. Aksay, and Y. Lin, "Graphene based electrochemical sensors and biosensors: a review," *Electroanalysis*, vol. 22, no. 10, pp. 1027–1036, 2010.

[9] N. A. H. Castro, "The electronic properties of graphene," *Vacuum*, vol. 83, no. 10, pp. 1248–1252, 2007.

[10] J. W. Yan, K. M. Liew, and L. H. He, "Free vibration analysis of single-walled carbon nanotubes using a higher-order gradient theory," *Journal of Sound and Vibration*, vol. 332, no. 15, pp. 3740–3755, 2013.

[11] N. Yao and V. Lordi, "Young's modulus of single-walled carbon nanotubes," *Journal of Applied Physics*, vol. 84, no. 4, pp. 1939–1943, 1998.

[12] Y. Zhang, L. W. Zhang, K. M. Liew, and J. L. Yu, "Free vibration analysis of bilayer graphene sheets subjected to in-plane magnetic fields," *Composite Structures*, vol. 144, pp. 86–95, 2016.

[13] M. Mirparizi and F. Aski, "Interlayer shear effect on vibrational behavior of bilayer graphene using the molecular mechanics simulation," *Propulsion and Power Research*, vol. 5, no. 3, pp. 250–260, 2016.

[14] S. O. Gajbhiye and S. P. Singh, "Multiscale nonlinear frequency response analysis of single-layered graphene sheet under impulse and harmonic excitation using the atomistic finite element method," *Journal of Physics D: Applied Physics*, vol. 48, no. 14, Article ID 145305, 2015.

[15] B. Arash and Q. Wang, "A review on the application of nonlocal elastic models in modeling of carbon nanotubes and graphenes," *Computational Materials Science*, vol. 51, no. 1, pp. 303–313, 2012.

[16] K. Behfar and R. Naghdabadi, "Nanoscale vibrational analysis of a multi-layered graphene sheet embedded in an elastic medium," *Composites Science and Technology*, vol. 65, no. 7-8, pp. 1159–1164, 2005.

[17] K. Behfar, P. Seifi, R. Naghdabadi, and J. Ghanbari, "An analytical approach to determination of bending modulus of a multi-layered graphene sheet," *Thin Solid Films*, vol. 496, no. 2, pp. 475–480, 2006.

[18] F. Yang, A. C. M. Chong, D. C. C. Lam, and P. Tong, "Couple stress based strain gradient theory for elasticity," *International Journal of Solids and Structures*, vol. 39, no. 10, pp. 2731–2743, 2002.

[19] P. Lu, L. H. He, H. P. Lee, and C. Lu, "Thin plate theory including surface effects," *International Journal of Solids and Structures*, vol. 43, no. 16, pp. 4631–4647, 2006.

[20] N. A. Fleck and J. W. Hutchinson, "Strain gradient plasticity," *Advances in Applied Mechanics*, vol. 33, pp. 295–361, 1997.

[21] P. Malekzadeh, A. R. Setoodeh, and A. A. Beni, "Small scale effect on the thermal buckling of orthotropic arbitrary straight-sided quadrilateral nanoplates embedded in an elastic medium," *Composite Structures*, vol. 93, no. 8, pp. 2083–2089, 2011.

[22] A. M. Zenkour and M. Sobhy, "Nonlocal elasticity theory for thermal buckling of nanoplates lying on Winkler-Pasternak elastic substrate medium," *Physica E: Low-dimensional Systems and Nanostructures*, vol. 53, pp. 251–259, 2013.

[23] M. Mohammadi, A. Farajpour, A. Moradi, and M. Ghayour, "Shear buckling of orthotropic rectangular graphene sheet embedded in an elastic medium in thermal environment This article is dedicated to Professor Hossien Mohammadi (Amir Hossien Mohammadi) on the occasion of his 60th birthday," *Composites Part B: Engineering*, vol. 56, pp. 629–637, 2014.

[24] J. Peddieson, G. R. Buchanan, and R. P. McNitt, "Application of nonlocal continuum models to nanotechnology," *International Journal of Engineering Science*, vol. 41, no. 3–5, pp. 305–312, 2003.

[25] W. H. Duan and C. M. Wang, "Exact solutions for axisymmetric bending of micro/nanoscale circular plates based on nonlocal plate theory," *Nanotechnology*, vol. 18, no. 38, Article ID 385704, 2007.

[26] S. Dastjerdi and M. Jabbarzadeh, "Non-linear bending analysis of multi-layer orthotropic annular/circular graphene sheets embedded in elastic matrix in thermal environment based on non-local elasticity theory," *Applied Mathematical Modelling*, vol. 41, pp. 83–101, 2017.

[27] K. M. Liew, X. Q. He, and S. Kitipornchai, "Predicting nanovibration of multi-layered graphene sheets embedded in an elastic matrix," *Acta Materialia*, vol. 54, no. 16, pp. 4229–4236, 2006.

[28] L. W. Zhang, Y. Zhang, and K. M. Liew, "Vibration analysis of quadrilateral graphene sheets subjected to an in-plane magnetic field based on nonlocal elasticity theory," *Composites Part B: Engineering*, vol. 118, pp. 96–103, 2017.

[29] S. C. Pradhan and J. K. Phadikar, "Small scale effect on vibration of embedded multilayered graphene sheets based on nonlocal continuum models," *Physics Letters A*, vol. 373, no. 11, pp. 1062–1069, 2009.

[30] S. R. Asemi, A. Farajpour, M. Borghei, and A. H. Hassani, "Thermal effects on the stability of circular graphene sheets via nonlocal continuum mechanics," *Latin American Journal of Solids and Structures*, vol. 11, no. 4, pp. 704–724, 2013.

[31] S. R. Asemi, M. Mohammadi, and A. Farajpour, "A study on the nonlinear stability of orthotropic singlelayered graphene sheet based on nonlocal elasticity theory," *Latin American Journal of Solids and Structures*, vol. 11, no. 9, pp. 1541–1564, 2014.

[32] W. Zhang and X. Wang, "Elastoplastic buckling analysis of thick rectangular plates by using the differential quadrature method,"

Computers & Mathematics with Applications, vol. 61, no. 1, pp. 44–51, 2011.

[33] Y. Huang and Q.-Z. Luo, "A simple method to determine the critical buckling loads for axially inhomogeneous beams with elastic restraint," *Computers & Mathematics with Applications*, vol. 61, no. 9, pp. 2510–2517, 2011.

[34] R. Ansari, R. Rajabiehfard, and B. Arash, "Nonlocal finite element model for vibrations of embedded multi-layered graphene sheets," *Computational Materials Science*, vol. 49, no. 4, pp. 831–838, 2010.

[35] L. W. Zhang, Y. J. Deng, and K. M. Liew, "An improved element-free Galerkin method for numerical modeling of the biological population problems," *Engineering Analysis with Boundary Elements*, vol. 40, pp. 181–188, 2014.

[36] K. M. Liew, Z. X. Lei, J. L. Yu, and L. W. Zhang, "Postbuckling of carbon nanotube-reinforced functionally graded cylindrical panels under axial compression using a meshless approach," *Computer Methods Applied Mechanics and Engineering*, vol. 268, pp. 1–17, 2014.

[37] Z. X. Lei, K. M. Liew, and J. L. Yu, "Free vibration analysis of functionally graded carbon nanotube-reinforced composite plates using the element-free kp-Ritz method in thermal environment," *Composite Structures*, vol. 106, pp. 128–138, 2013.

[38] Y. Zhang, Z. X. Lei, L. W. Zhang, K. M. Liew, and J. L. Yu, "Nonlocal continuum model for vibration of single-layered graphene sheets based on the element-free kp-Ritz method," *Engineering Analysis with Boundary Elements*, vol. 56, pp. 90–97, 2015.

[39] Z. Wu, F. Hu, Y. Zhang, Q. Gao, and Z. Chen, "Mechanical analysis of double-layered circular graphene sheets as building material embedded in an elastic medium," *Journal of Central South University*, vol. 24, no. 11, pp. 2717–2724, 2017.

[40] PL. Pasternak, *On a New Method of Analysis of an Elastic Foundation by Means of Two Foundation Constants, Gosudarstvennoe Izdatelstvo Literaturi Po Stroitelstvu I Arkhitekture, Moscow*, 1954.

[41] E. Jomehzadeh, A. R. Saidi, and N. M. Pugno, "Large amplitude vibration of a bilayer graphene embedded in a nonlinear polymer matrix," *Physica E: Low-dimensional Systems and Nanostructures*, vol. 44, no. 10, pp. 1973–1982, 2012.

[42] J.-S. Chen, C. Pan, C.-T. Wu, and W. K. Liu, "Reproducing kernel particle methods for large deformation analysis of nonlinear structures," *Computer Methods Applied Mechanics and Engineering*, vol. 139, no. 1-4, pp. 195–227, 1996.

[43] X. Q. He, S. Kitipornchai, and K. M. Liew, "Resonance analysis of multi-layered graphene sheets used as nanoscale resonators," *Nanotechnology*, vol. 16, no. 10, pp. 2086–2091, 2005.